Silk-based multilayered angle-ply annulus fibrosus construct to recapitulate form and function of the intervertebral disc

Bibhas K. Bhunia[a], David L. Kaplan[b,1], and Biman B. Mandal[a,1]

[a]Biomaterial and Tissue Engineering Laboratory, Department of Biosciences and Bioengineering, Indian Institute of Technology Guwahati, Guwahati 781039, India; and [b]Department of Biomedical Engineering, Tufts University, Medford, MA 02155

Edited by Robert Langer, Massachusetts Institute of Technology, Cambridge, MA, and approved December 6, 2017 (received for review September 16, 2017)

Recapitulation of the form and function of complex tissue organization using appropriate biomaterials impacts success in tissue engineering endeavors. The annulus fibrosus (AF) represents a complex, multilamellar, hierarchical structure consisting of collagen, proteoglycans, and elastic fibers. To mimic the intricacy of AF anatomy, a silk protein-based multilayered, disc-like angle-ply construct was fabricated, consisting of concentric layers of lamellar sheets. Scanning electron microscopy and fluorescence image analysis revealed cross-aligned and lamellar characteristics of the construct, mimicking the native hierarchical architecture of the AF. Induction of secondary structure in the silk constructs was confirmed by infrared spectroscopy and X-ray diffraction. The constructs showed a compressive modulus of 499.18 ± 86.45 kPa. Constructs seeded with porcine AF cells and human mesenchymal stem cells (hMSCs) showed ∼2.2-fold and ∼1.7-fold increases in proliferation on day 14, respectively, compared with initial seeding. Biochemical analysis, histology, and immunohistochemistry results showed the deposition of AF-specific extracellular matrix (sulfated glycosaminoglycan and collagen type I), indicating a favorable environment for both cell types, which was further validated by the expression of AF tissue-specific genes. The constructs seeded with porcine AF cells showed ∼11-, ∼5.1-, and ∼6.7-fold increases in col Iα *1*, sox 9, and aggrecan genes, respectively. The differentiation of hMSCs to AF-like tissue was evident from the enhanced expression of the AF-specific genes. Overall, the constructs supported cell proliferation, differentiation, and ECM deposition resulting in AF-like tissue features based on ECM deposition and morphology, indicating potential for future studies related to intervertebral disc replacement therapy.

silk | annulus fibrosus | intervertebral disc | biomaterials | tissue engineering

Intervertebral disc degeneration (IDD) is the major cause of lower back pain and limited mobility, contributing significantly to health-care expenditures (1). IDD is characterized by progressive damage to the annulus fibrosus (AF) region which confines the gelatinous nucleus pulposus (NP). This damage to AF is associated with mechanical stress, loss of function, biological remodeling, and dehydration of inner NP extracellular matrix. Current therapeutic treatments for IDD include conservative methods, such as medication and physical therapy, or surgical intervention, including spinal fusion and total disc arthroplasty. However, these surgical procedures are only effective in symptomatic pain relief without restoring the biomechanical functions of the intervertebral disc (IVD), which may lead to disintegration of adjacent segments. Furthermore, these surgical procedures are case-dependent and cannot be applied to all patients (1). In this context, tissue engineering technology provides a promising alternative strategy for the treatment of IDD through implantation of in vitro-engineered tissue discs mimicking native structure and functions.

Tissue engineers continue to develop biomimetic tissue constructs with combinations of various biomaterials and engineered designs to recapitulate AF structure and function essential for regeneration (2). The replication of the anatomic forms of AF using different biomaterials has included both natural and synthetic polymers; however, few studies have focused on recapitulation of structural features of the tissue. Most importantly, the introduction of lamellar scaffolds in AF tissue engineering may be critical for the field due to the direct relationship between the hierarchical features and mechanical functions of the tissue (3). One study involved the fabrication of alginate/chitosan scaffolds to form a lamellar AF structure that supported canine AF cell growth and function (4). Biphasic scaffolds such as demineralized bone matrix gelatin poly(polycaprolactonetriol malate) supported the regeneration of AF tissue, structurally and mechanically close enough to native rabbit AF (5). Similarly, silk-based lamellar constructs have also been fabricated for AF tissue engineering. A biphasic construct consisting of silk fibroin (SF)-based porous lamellar structures for AF in combination with fibrin/hyaluronic acid gels for the NP region were reported (6). In an advanced strategy, silk fiber-based multilamellar constructs were prepared in which silk fibers or chondroitin sulfate-modified silk fibers were wound to form a hierarchical and lamellar structure resembling native AF tissue (7–9). However, the degradation rate of natural silk fibers was very slow and was a constraint in the study, limiting replacement by neotissue (10). In silk-based tissue engineering, silk fibers are often regenerated and then processed into different formats, namely scaffolds, films, mats, or hydrogels, before use as implants. Consequently, the biodegradation of these regenerated SF products is faster than that of native silk fibers, both in vitro and in vivo (11). Another

Significance

In this study we have developed a fabrication procedure for a silk-based bioartificial disc adopting a directional freezing technique. The fabricated biodisc mimicked the internal intricacy of the native disc as evaluated by electron microscopy. The mechanical properties of these biodiscs were similar to those of the native ones. The fabricated biodiscs supported primary annulus fibrosus or human mesenchymal stem cell proliferation, differentiation, and deposition of a sufficient amount of specific ECM. A small unit of the construct was implanted subcutaneously to show its negligible immune response. The success here means that the silk-based bioartificial disc can be a promising strategy for future direction toward disc replacement therapy.

Author contributions: B.K.B., D.L.K., and B.B.M. designed research; B.K.B. and B.B.M. performed research; B.K.B., D.L.K., and B.B.M. analyzed data; and B.K.B., D.L.K., and B.B.M. wrote the paper.

The authors declare no conflict of interest.

This article is a PNAS Direct Submission.

Published under the PNAS license.

[1]To whom correspondence may be addressed. Email: biman.mandal@iitg.ernet.in or david.kaplan@tufts.edu.

This article contains supporting information online at www.pnas.org/lookup/suppl/doi:10.1073/pnas.1715912115/-/DCSupplemental.

Downloaded at Palestinian Territory, occupied on December 7, 2021

www.manaraa.com

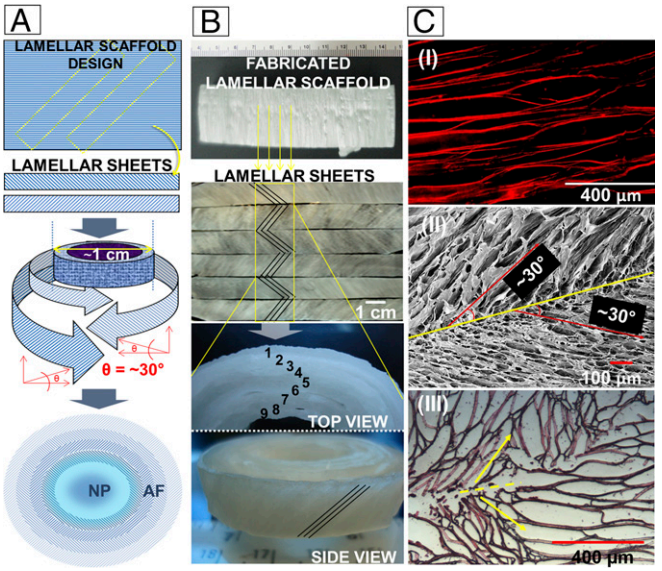

Fig. 1. (*A*) Schematic representation of multilayered disc-like angle-ply construct preparation. (*B*) Images showing stepwise fabrication of the disc. (*C*) Images showing basic features of the lamellar construct: (*I*) fluorescent image of lamellar alignment and (*II* and *III*) the cross-aligned pattern reveled by SEM and histological section, respectively.

approach to address the complex hierarchical design of AF is electrospinning, which has been previously introduced to engineer various aligned tissues (12). In this technique, the fabricated constructs exhibit highly aligned arrays of polymeric nanofibers that mimic the natural organization of different fiber-reinforced soft tissues, including the AF (13). Multiscale, biologic constructs using electrospun mats of polycaprolactone that were hierarchically and anatomically relevant to the native AF were reported (13). However, electrospun scaffolds often face a number of limitations including low porosity that restricts uniform cell infiltration and a discrepancy of mechanical properties compared with native AF.

The multiscale, hierarchical, collagen fiber-reinforced composite structure of the AF is responsible for shock absorption and flexibility of the spinal column. The AF consists of 15–25 concentric layers; each layer is strengthened by collagen nanofibers which are aligned at a ~30° angle with respect to the diagonal plane of the spine axis, but in alternate directions in each successive layer (2). This type of organization creates an angle-ply structure which is critical for proper biochemical and biomechanical functioning of the AF. Understanding such intricate organization is key to recent efforts to simulate anatomical features for a physiologically functional engineered disc.

In the present study SF was used for the fabrication of lamellar 3D scaffolds. To mimic the complex organization of AF anatomy, silk-based disc-like angle-ply constructs that consisted of concentric layers of lamellar sheets were prepared. The lamellar alignment represented the alternate direction of lamellae in successive layers of native AF, making an angle-ply structure. A directional freezing technique was adopted to prepare the lamellar scaffolds as we described previously (14). Mechanical properties, the impact of fiber alignment on cell proliferation, extracellular matrix secretion [sulfated glycosaminoglycan (sGAG) and collagen content analysis], and specific gene expression (through real-time PCR) of AF cells and human mesenchymal stem cells (hMSCs) seeded on these scaffolds were addressed in the study.

Results

Scaffold Features. To replicate the gross anatomic form of the IVD a two-step approach was adapted; first, lamellar scaffolds were fabricated, and then a disc-like angle-ply construct was prepared with the lamellar sheets. Lamellar scaffolds were fabricated by unidirectional freezing of 5% (wt/vol) aqueous SF solution (Fig. S1*B*). In our previous study we reported the detailed procedures for the preparation of lamellar scaffolds and their use in cellular response studies with chondrocytes and bone marrow-derived hMSCs (14). In the present study we implemented that strategy to prepare disc-like angle-ply constructs. To mimic the multilamellar hierarchy of AF anatomy, the predesigned SF sheets with the lamellar alignment with an angle of ~30° to its vertical axis were wrapped concentrically around a mold of ~1 cm in diameter, but in opposing directions (+30° and −30°) of successive layers to form an angle-ply arrangement of the lamellae (Fig. 1 *A* and *B*). The cross-aligned structure was confirmed by scanning electron microscope (SEM) and histological sectioning of the construct (Fig. 1 *C*, *II* and *III*).

With the help of SEM and fluorescence image analysis the distance between two adjacent lamellae (i.e., interlamellar distance) and the lamellar channel length were determined and found to be in the range of 62–116 μm and 167–393 μm, respectively (Figs. 1 *C*, *I* and 2*A*). The transverse section of scaffolds showed the circular opening of lamellar channels had pore sizes ranging from 44 to 78 μm (Fig. 2*A*). Cell-seeded scaffolds showed lamellar alignment of cells inside the lamellar pores (Fig. 2*B*). The degree of crystallinity and secondary structure (i.e., β-sheet) of the lamellar constructs were confirmed by wide-angle X-ray diffraction (WAXD) and FTIR analysis. In WAXD analysis, two X-ray diffraction peaks were observed at 2θ = 21° (major peak) and 24° (minor peak) with a shoulder peak at 41° (Fig. 2*C*), confirming the crystalline state of the protein in the scaffolding. FTIR spectroscopy data showed the β-sheet conformational transitions of silk with the signature peaks at 1,641, 1,519, and 1,231 cm^{-1} for amide I, II, and III, respectively (Fig. 2*D*).

Mechanical Properties of Constructs. Assessment of mechanical properties is a critical aspect for load-bearing tissue engineered constructs. For the compressive study, three sets of acellular constructs and one set of native tissue were considered; set I consisted of only multilayered angle-ply AF construct, set II was

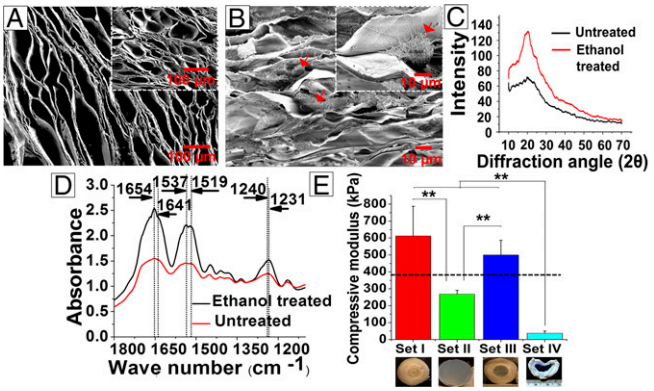

Fig. 2. Physical characterizations of lamellar construct. (*A*) SEM images showing the lamellar alignment of pores and its cross-sections with circular pores (*Inset*). (*B*) The cell-seeded scaffolds where cells are aligned in a lamellar way (red arrows) and a magnified image (*Inset*). (*C* and *D*) WAXD and FTIR analysis of the construct, respectively. (*E*) Mechanical properties of fabricated disc; three different sets of acellular constructs were investigated for the compressive modulus study. Set IV was the porcine native AF. The dashed line indicates native human AF benchmark (15). Data represent mean ± SD ($n = 3$), where $^{**}P \leq 0.01$. (Scale bars: 100 μm for *A* and 10 μm for *B*.)

Downloaded at Palestinian Territory, occupied on December 7, 2021
www.manaraa.com

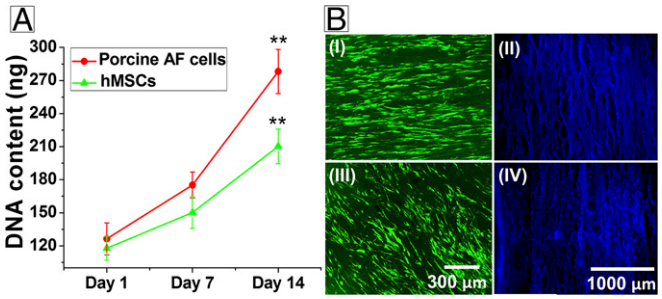

Fig. 3. (*A*) Cell proliferation (porcine AF cells and hMSCs) within lamellar construct over 2 wk. (*B*) Confocal imaging of cells; *I* and *II* represent live cell staining (using calcein AM, green color) and nucleus staining (using Hoechst 33342, contrast blue dots) for porcine AF cells, and *III* and *IV* show the same for hMSCs. Data represent mean ± SD ($n = 3$), where $^{**}P \leq 0.01$.

2% agarose gel as the replica of NP gel, set III was the combination of both as a prototype of whole IVD, and set IV was native porcine AF tissue (Fig. 2*E*). The maximum compressive modulus (612.14 ± 175.48 kPa) was measured for set I, a compact multilayered angle-ply AF construct devoid of an NP zone in the middle, while set III representing the whole IVD showed a value of 499.18 ± 86.45 kPa. The compressive modulus (268.52 ± 21.6 kPa) was significantly less for 2% agarose ($P \leq 0.01$), a replica of the NP region, compared with others. The least compressive modulus (37.45 ± 12.79 kPa) was calculated for native porcine AF. The value was in line with findings in a previous report (16). All tests were performed under hydrated conditions (in PBS, pH 7.4 and 37 °C) to mimic the physiological microenvironment.

Cell Survival, Proliferation, and Alignment Study. Cytocompatibility and cellular viability are vital for tissue engineering applications. Isolated porcine primary AF cells and hMSCs were cultured within the lamellar constructs for in vitro assessments of cellular viability, proliferation, and arrangement. Both types of cell-seeded lamellar constructs were maintained in culture medium for 2 wk. Based on florescence image analysis, the attachment and alignment of cells within lamellar scaffolds were studied. Cell viability was evaluated by live/dead assay kit (Fig. 3 *B*, *I* and *III*) and the cellular arrangement was studied by Hoechst 33342 staining for nuclei (Fig. 3 *B*, *II* and *IV*). Cells were evenly distributed, confluent, and aligned in a lamellar morphology for both cases (porcine AF cells and hMSCs) after 2 wk of culture.

For cell proliferation, total DNA content was evaluated on days 1, 7, and 14 (Fig. 3*A*). Equal numbers of both cells (porcine AF cells and hMSCs) were seeded to the separate lamellar constructs and continued for 14 d. On the basis of PicoGreen DNA assay, an increased proliferation rate was observed for porcine AF cells compared with hMSCs at each time point. Porcine AF cells proliferated with the increase of ∼1.4- and ∼2.2-fold at days 7 and 14, respectively, compared with initial cell number at day 1 ($P \leq 0.01$). Similarly, ∼1.26- and ∼1.7-fold increases in cell proliferation at days 7 and 14, respectively, were observed for the hMSCs ($P \leq 0.01$). The maximum DNA content for porcine AF cells reached 282.35 ± 14.68 ng compared with hMSCs (211.54 ± 13.55 ng) at day 14.

Histology and Immunohistochemistry Analysis. From histology and immunohistochemistry analysis the cellular distribution and ECM deposition within the tissue engineered constructs was assessed. For histological analysis, cell-seeded lamellar constructs were sectioned and stained with H&E. The results showed that cells (in both cases: porcine AF cells and differentiated hMSCs) were homogeneously distributed throughout the constructs and arranged in a lamellar fashion, attaching to the lamellar walls after 2 wk of culture (Fig. 4 *A* and *D*). For the identification of AF-specific ECM deposition, Alcian blue staining (for sulfated GAGs) and immunohistochemistry (for type I collagen) were performed. Alcian blue staining revealed even deposition of sGAG within the entire lamellar constructs for both cases, but with more intense blue color for porcine AF cell-seeded constructs (Fig. 4 *B* and *E*). Similarly, from immunohistochemistry, type I collagen was secreted abundantly by both cells (i.e., porcine AF cells and differentiated hMSCs) after 2 wk of culture in chondrogenic medium (Fig. 4 *C* and *F*).

Quantitative Analysis of ECM Deposition. Alcian blue staining for sGAG and immunohistochemistry for type I collagen was further supported by the quantitative biochemical analysis suggesting ECM secretion by both porcine AF cells and differentiated hMSCs in chondrogenic medium. Both collagen and sGAG deposition increased with time for both cell types, but higher values were obtained for the porcine AF cells. For type I collagen from porcine AF cells, the values increased to ∼3.6-fold and ∼9.8-fold at days 7 and 14, respectively, compared with the initial seeding ($P \leq 0.01$). Similarly, for differentiated hMSCs, a ∼3.4- and ∼13.4-fold increase in collagen secretion was monitored at days 7 and 14, respectively, compared with day 1 ($P \leq 0.01$). The amount of total collagen content per unit scaffold mass was higher in the case of porcine AF compared with the differentiated hMSCs at each time frame (days 3, 7, and 14). The maximum collagen content per milligram of scaffold for porcine AF cells was 70.88 ± 15.96 μg (∼54% of native porcine AF tissue) at day 14, whereas for differentiated hMSCs the value reached 49.9 ± 7.8 μg (Fig. 5*A*). Similarly, sGAG (scaffold and media) content for porcine AF cells showed higher values than hMSCs at each time point (days 3, 7, and 14). For porcine AF cells, the value increased to ∼10.2- and ∼44.1-fold at days 7 and 14, respectively, compared with day 1 ($P \leq 0.01$). In the case of differentiated hMSCs, a similar value was obtained (∼10-fold for day 7 and ∼44.8-fold for day 14). However, compared with the total amount of sGAG content per unit mass of scaffolds, the value (12.1 ± 5.3 μg) was much lower than that of porcine AF cells (22.08 ± 7.02 μg, ∼55% of native porcine AF tissue) (Fig. 5*B*).

Real-Time PCR Analysis. In further support of qualitative (histology and immunohistochemistry) and quantitative (biochemical analysis) assessments, transcript levels of AF-related marker genes (Col I*α 1*, aggrecan, and sox-9) were assessed by real-time PCR. For porcine AF cells the mRNA expression level of the three genes increased with the time (days 7 and 14), and the maximum expression was observed for Col I*α 1* when maintained in chondrogenic medium (Fig. 5*C*). The expression level of Col I*α 1* increased ∼4.3- and ∼11-fold at days 7 and 14, respectively, compared with day 1 ($P \leq 0.01$). Relatively lower levels of expression were observed for both sox-9 and aggrecan genes. The level of expression

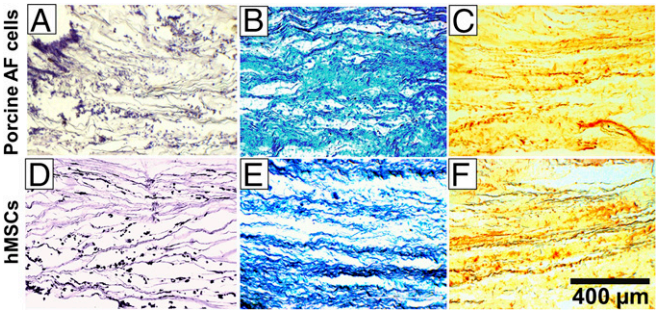

Fig. 4. Histology and immunohistochemistry of lamellar constructs over 2 wk of culture in chondrogenic medium. (*A*–*C*) Images represent porcine AF cell-seeded constructs. (*D*–*F*) Images represent hMSC-seeded constructs. *A* and *D* for H&E staining show cellular distribution within the lamellar constructs, *B* and *E* show Alcian blue staining for sGAG deposition, and *C* and *F* show immunostaining of deposited collagen I.

Downloaded at Palestinian Territory, occupied on December 7, 2021
ENGINEERING
MEDICAL SCIENCES
www.manaraa.com

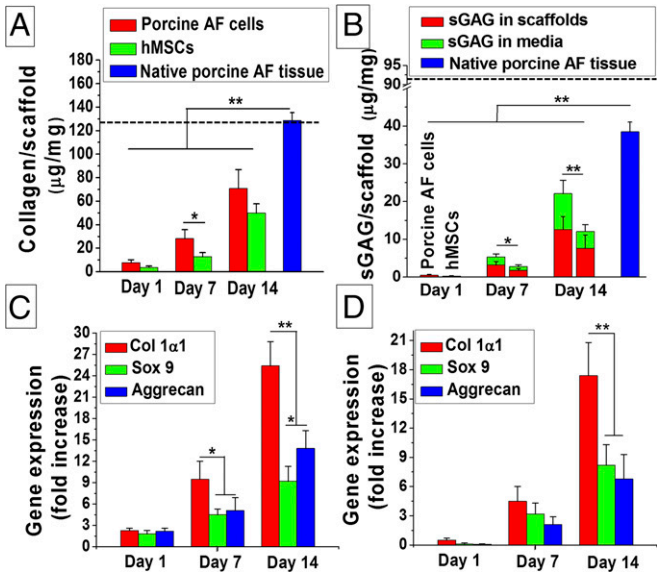

Fig. 5. Biochemical analysis of cell seeded lamellar constructs. (*A*) Collagen content analysis and (*B*) sGAG deposition within lamellar scaffolds. The dashed line indicates native human AF benchmark (17). Gene expression study for (*C*) AF cells and (*D*) hMSCs in time points of days 1, 7, and 14 cultured in chondrogenic media. Data represent mean ± SD ($n = 3$), where $*P \leq 0.05$ and $**P \leq 0.01$.

for both sox-9 and aggrecan genes increased ∼5.1- and ∼6.7-fold, respectively, at day 14 compared with day 1.

The hMSCs showed increased levels of AF tissue-specific gene expression (Col I*α 1*, sox-9, and aggrecan) with time (Fig. 5*D*). Similar to the porcine AF cells, maximum expression was observed for Col I*α 1* in differentiated hMSCs at any time point taken. It was observed that the Col I*α 1* gene was expressed with an increase of ∼9- and ∼34.8-fold at days 7 and 14, respectively, compared with day 1 ($P \leq 0.01$).

In Vivo Assessments. In vivo implantation of the tissue engineered constructs helps to evaluate the biomaterial integration and immune responses. To understand the immune response, the lamellar constructs were implanted s.c. in mice and retrieved at weeks 1 and 4, followed by H&E and immunofluorescence staining for macrophages (Fig. 6). After 1 wk, the retrieved constructs showed immune cells (mainly macrophages, confirmed by immunofluorescence for CD68) surrounding the constructs (Fig. 6 *B*, *II*). Few macrophages infiltrated the scaffolds. Aggregation of macrophages followed by fibroblast layers was also observed surrounding the implanted scaffolds and no sign of tissue necrosis was found. Following 4 wk, the retrieved scaffolds showed negligible infiltration of immune cells inside the implanted scaffolds (Fig. 6 *C*, *II*). Scaffold–native tissue integration was also clearly visualized, and negligible degradation of the lamellar constructs was observed over the 4 wk.

Discussion

Disc-Like Angle-Ply Construct Fabrication. Repairing fibrocartilaginous tissues like AF of IVDs is a challenging task. The intricacy arises due to the avascular nature, low cellularity that limits regeneration, and the hierarchical structural organization of the tissue that dictates its biomechanical properties. To address such challenges, a cross-aligned scaffold construct that mimics the native tissue architecture and mechanical properties was developed. In our previous study we assessed the influence of silk-based lamellar scaffolds prepared using directional freezing in adipogenic and chondrogenic differentiation of hMSCs (14). Directional freezing is based on a simple thermodynamic principle where the velocity and morphology of the ice-front propagation is controlled through the sample in a unique direction. Moreover, use of an aqueous-based polymeric system (where water is the main sol fraction) avoids the introduction of any toxic products into the scaffolds. In the present study we implemented this technique to prepare lamellar scaffolds with multilamellar angle-ply constructs to mimic native disc morphology. The process was conducted in two steps: preparing lamellar scaffolds followed by excising rectangular sheets possessing ∼30° angle of lamellar directions to the vertical axis and then encircling them in alternate directions so that the assembled structure had a disc-like angle-ply construction (Fig. 1 *A* and *B*). To prepare lamellar scaffolds, a polydimethylsiloxane (PDMS) mold was used, consisting of two hollow chambers divided by a copper metal plate. PDMS, a transparent silicon polymer, offers good thermal and chemical stability, electrical resistivity, and mechanical flexibility but also has poor thermal conductivity (0.15 $W \cdot m^{-1} \cdot K^{-1}$) (18). In contrast, the copper plate used as the divider has high thermal conductivity (401 $W \cdot m^{-1} \cdot K^{-1}$). The ratio of thermal conductivity of these two components is 2,673.3; thus, directional ice crystal formation rate was rapid and originated from the metal plate surface rather than the PDMS walls (Fig. S1).

Physicochemical Characterization. The regenerated *Bombyx mori* SF typically exhibits random coil and β-turn (without α-helix), termed silk I. Upon exposure to 70% (vol/vol) ethanol, silk I is converted to silk II due to induction of β-sheet crystals. After lyophilization, the lamellar constructs were subjected to ethanol treatment to induce crystallinity to ensure stability in aqueous medium. Following treatment with ethanol, conformational transition occurred to silk II as previously reported (Fig. 2*D*) (14, 19). Similarly, the WAXD data supported crystallinity of the lamellar constructs (Fig. 2*C*).

SEM and fluorescent-based image analysis revealed the cross-aligned and lamellar characteristics of the constructs (Figs. 1 *C*, *I* and *II* and 2*A*). Porosity and pore size of lamellar scaffolds are mainly governed by lamellar distance and channel length. Gas perfusion and nutrient exchange during culture depend on pore size and porosity of the scaffolds and influence cell survival, proliferation, and differentiation. We previously reported the effect of SF concentration on interlamellar distance and its porosity (14). Electron microscopy of the transverse sections of the scaffolds revealed circular openings (44 to 78 μm) of the lamellar channels. These openings were the result of longitudinal ice crystal propagation at the time of rapid freezing in liquid N_2. SEM also supported the homogeneous and aligned cell distribution throughout the lamellar channels.

Biomechanics. The complex architecture and composition make AF an anisotropic, nonlinear, and viscoelastic tissue to bear mechanical loads. Although AF is subjected to various types of

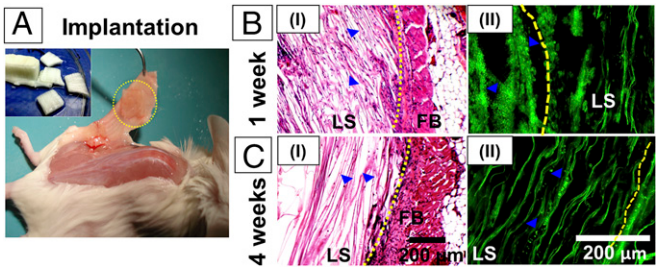

Fig. 6. In vivo assessment of lamellar constructs. (*A*) Retrieval of lamellar construct from s.c. pocket of mice after 4 wk of implantation. H&E staining of implants after 1 wk (*B*, *I*) and 4 wk (*C*, *I*). Immunofluorescence of CD68 for macrophages infiltration in the implanted scaffolds after 1 wk (*B*, *II*) and 4 wk (*C*, *II*). Yellow dotted line represents scaffold–tissue interface. Filled blue triangle show the macrophage (green dots) infiltration inside implants. FB, fibroblast layers; LS, lamellar scaffold.

Downloaded at Palestinian Territory, occupied on December 7, 2021
www.manaraa.com

mechanical forces, including uniaxial and biaxial tension, shear, and torsion, compressive properties were assessed for the designed multilayered angle-ply constructs. Under compressive loading the disks become narrow in height and bulge in an outward direction, experiencing both axial and radial compressive stress. Despite the high ductility and stiffness of silk fibers, mechanical properties of the final products depend on postprocessing and fabrication procedures. For the compressive study, three sets of scaffolds were used (Fig. 2*E*). Set I scaffolds showed the highest compressive modulus (>600 kPa) due to the highly compact nature of the scaffold. However, this type of compact structure cannot be applied for disc replacement therapy as it does not contain an NP region. Set II consisted of only agarose gel (2 wt % wt/vol) and showed the least compressive modulus (~270 kPa). Better mechanical properties were registered for set III that represented the whole disc, consisting of concentric rings of lamellar constructs surrounding the gelatinous NP substitute (agarose gel). This observation indicated the interaction between these two regions prompts a mechanical response in compression that emulated the native disc. This type of construct provided a compressive modulus of 499.18 ± 86.45 kPa, a value in the range of the compressive modulus of native human AF tissues (380 ± 160 kPa) (15). Thus, at this juncture, the assessment of tensile strength, shear stress, and other mechanics would be required to support final designs related to the biomechanical functionality of the disc.

Cytocompatibility Study. Cytocompatibility of a biomaterial for tissue engineering is also a key factor for its clinical success. Cellularity often depends on a "form follows function" rule where scaffolds act as functional templates to guide cellular remodeling (20). Porous scaffolds used for AF tissue engineering supported nonuniform and reduced cell proliferation in comparison with lamellar scaffolds (3). SF is widely accepted for various regenerative applications due to its versatile features including high strength, biocompatibility, and biodegradability with low immunogenicity (21). In this study, cellular compatibility of the constructs was assessed with two types of cells: porcine primary AF cells and bone marrow-derived hMSCs. AF cells proliferated and formed ECM related to the vertebral disc. The potential use of AF cells in IVD tissue engineering has also been reported previously (3). Complications in the isolation and lack of sufficient donors limit the use of primary cells for implantable scaffolds. This has stimulated interest toward alternative cell sources, such as stem cells. MSCs are multipotent stromal cells that have the ability to differentiate into various lineages including osteoblast, myocytes, adipocytes, and chondrocytes. MSCs have shown significant contributions in IVD tissue engineering (22). MSCs may be exploited either in their undifferentiated stage, allowing them to differentiate in vivo influenced by local stimulus, or in their differentiated stage in vitro before implantation. In the former case, unwanted differentiation may occur in the injury site, whereas differentiated MSCs are phenotypically stable and resistant to transdifferentiation when maintained in chondrogenic media (23). In this context, bone marrow-derived hMSCs were isolated and allowed to differentiate into the chondrogenic lineage after seeding into the angle-ply constructs in the present study. Cell-seeded constructs were maintained for 2 wk and cellularity was checked by DNA content (Fig. 3*A*). Both cell sources proliferated in the construct with time, and enhanced proliferation was observed for the primary AF cells. After 2 wk of culture in chondrogenic medium, AF cells showed ~2.2-fold proliferation from initial seeding ($P \leq 0.01$), whereas hMSCs showed a ~1.7-fold increase ($P \leq 0.01$). In contrast, the AF cells, which were already differentiated, maintained their normal phenotype and proliferation rate throughout the experiment. However, cell viability using calcein AM and nuclear staining by Hoechst 33342 revealed cellularity and alignment in the constructs (Fig. 3*B*).

Biochemical Study. A successful bioengineered construct supports cell attachment and proliferation and also supports the deposition of ECM for functional tissue. Biochemical analysis of constructs after 2 wk of culture in chondrogenic medium revealed significant accumulation of both collagen and sGAG, the two main ECM components of AF. The AF consists of ~67% of collagen in its dry weight, where type I collagen accounts for ~80% of total collagen content. Although proteoglycan content is as predominant in the outer AF regions, the amount gradually increases toward the central region. However, the proportion of collagen to proteoglycan changes throughout life and is also associated with disc degeneration. The developed angle-ply constructs supported both the primary AF cells and hMSCs and the AF cells secreted increased amounts of ECM components compared with the hMSCs (Fig. 5 *A* and *B*). The reason for this increased level of ECM secretion by the primary AF cell might be due to their highly differentiated state. This was further confirmed by gene expression, where increased levels of col I*α 1* and aggrecan were observed (Fig. 5 *C* and *D*). Similarly, differentiation of hMSCs in lamellar constructs was evident from the up-regulated expression of col I*α 1*, aggrecan, and sox 9 mRNA (early chondrogenic differentiation marker) in chondrogenic medium for 2 wk. The chondrogenic medium consists of ITS+ (insulin, transferrin, and selenious acid), TGF-β, and dexamethasone, the fundamental components for chondrogenic differentiation of MSCs. Previously it was reported that TGF-β induced new ECM synthesis in both old and degenerated discs (24). Enhanced cell proliferation has been reported under the combined effects of ITS+ and TGF-β, whereas dexamethasone exerted an augmentative and suppressive influence on protein and proteoglycans, respectively (25). We observed that decreased levels of aggrecan mRNA expression were associated with increased col I*α 1* gene expression by hMSCs compared with AF cells.

Cellular infiltration and their arrangement or specific ECM molecule deposition can be visualized by histological analysis of the tissue engineered constructs. H&E staining of the constructs revealed cellular infiltration and alignment in the lamellae (Fig. 4 *A* and *D*). sGAG is one of the predominant ECM molecules secreted by chondrocytes or differentiated stem cells (to chondrocytic lineage). Fibrochondrocytic in nature, AF cells secreted sGAGs in the lamellar constructs and an intense and homogeneous blue color appeared throughout the scaffold section. Similarly, deposition of sGAG by differentiated hMSCs in the lamellar construct was confirmed by Alcian blue staining (Fig. 4 *B* and *E*). Collagen type I, another hallmark ECM component of AF tissue, was detected by immunohistochemistry. Both the primary AF cells and hMSCs secreted, as corroborated by immunostaining for collagen type I (Fig. 4 *C* and *F*). However, the stained color was comparatively more intense (visual observation) for the constructs seeded with primary AF cells, supporting the biochemical and gene expression studies.

In Vivo Response. While the in vitro experiments assist in providing an insight into the cellular interactions with the materials, in vivo studies are relevant to understanding overall tissue responses. Any biomaterial which is nonautologous elicits some extent of foreign body response (FBR) following implantation. FBR also depends on biomaterial characteristics, including size, geometry, topology, and site of implantation (26). In this study, the constructs were s.c. implanted in mice and retrieved after 1 and 4 wk followed by H&E staining (Fig. 6). Although recruitment of macrophages was observed surrounding the implants after 1 wk, there was a significant reduction after 4 wk. Following 4 wk, the implanted constructs retained structural integrity, including the lamellar alignment. This observation is in line with previous studies that demonstrate lower inflammatory responses toward silk materials (14).

In the current study, recapitulation of AF internal architecture has been achieved using a tissue engineering approach, but it is necessary to address other formidable challenges for the clinical

Downloaded at Palestinian Territory, occupied on December 7, 2021

www.manaraa.com

implementation of the existing technologies. To move the current technology toward in vivo application it is critically important to ensure the integration of the implanted engineered disc to the surrounding tissue as well as the AF–NP confinement. The NP can be transplanted as a biphasic structure (set III) or can be injected in a minimally invasive way after AF transplantation. This is important as the high mechanical properties of the disc are attributed to its sealed confinement. Hence, the long-term aim would be the fabrication of an entire construct comprising AF, gelatinous NP, and superior–inferior end plate. The engineered disc can be implanted in a cellular or acellular state. For the cellular disc, it needs to be cultured in a dynamic bioreactor system for better tissue maturation. The current study focuses on the use of two different cell types, primary cells and hMSCs. The fabricated construct was validated by both cell types in terms of biocompatibility and tissue formation. So, the biological construct, upon implantation, mimicking the internal architecture will provide the mechanical properties, whereas the cellular part will prevent further degeneration by supporting the regenerative process. Despite of these obstacles in clinical implementation the current work may provide a better understanding about bioartificial disc preparation mimicking its hierarchical organization.

Conclusions

Structural recapitulation of AF tissue is a major challenge. We devised a strategy to address this by using a silk-based angle-ply approach. The construct mimics the native structure–function attributes of the disc and provides sufficient mechanical strength to function in load-bearing activities. The developed disc supported primary AF cell proliferation, alignment, and ECM deposition. Differentiation of hMSCs to chondrogenic lineage further supported the prospects for application of the constructs toward disc needs.

Materials and Methods

Fabrications of Disc-Like Angle-Ply Structure. The aqueous solution of SF was derived from *B. mori* silk cocoons according to the procedure previously described (14). The lamellar scaffolds were prepared using the protocol described in our previous work (Fig. S1) (14). Rectangular sheets having lamellar pores of ~30° angle to their length were encircled in alternating directions so they made an angle-ply construct (Fig. 1*A*).

Physicochemical and Biochemical Studies. The fabricated constructs were physicochemically characterized by SEM, WAXD, and FTIR followed by mechanical studies. Biological responses of constructs were checked using primary porcine AF and hMSCs. Histological analysis was performed to study the cellular distribution and ECM secretion pattern inside the cell-seeded constructs. DNA, sGAG, total collagen, and real-time gene expression for Col Iα1, sox-9, and aggrecan were performed following the manufacturer's protocol.

In Vivo Response Study. BALB/c mice were used to evaluate the in vivo immune response to the fabricated constructs. A small unit of lamellar construct was implanted into s.c. pocket. Inflammatory responses were checked at the end of 1 and 4 wk on the basis of H&E and CD68 immune staining for macrophages. All of the experiments were performed following protocols approved by the Tufts University Institutional Animal Care and Use Committee. A more detailed description is included in *SI Materials and Methods*.

Statistical Analysis. All quantitative experiments were performed at least in triplicate, and results were expressed as mean ± SD for $n = 3$ unless specified. Statistical analyses of data were performed by ANOVA. Differences between groups of $*P \leq 0.05$ are considered statistically significant and $**P \leq 0.01$ as highly significant.

ACKNOWLEDGMENTS. We thank Dr. Bruce Panilaitis for assistance during the in vivo testing. This work was supported by the Government of India through Department of Science and Technology Grants SB/EMEQ-024/2013 and IFA-13 LSBM-60 and Department of Biotechnology Grants BT/548/NE/U-Excel/2014 and BT/IN/Sweden/38/BBM/2013 (to B.B.M.) and a scholarship from the Ministry of Human Resource Development, Government of India (to B.K.B.).

1. Guterl CC, et al. (2013) Challenges and strategies in the repair of ruptured annulus fibrosus. *Eur Cell Mater* 25:1–21.
2. Nerurkar NL, Elliott DM, Mauck RL (2010) Mechanical design criteria for intervertebral disc tissue engineering. *J Biomech* 43:1017–1030.
3. Park SH, et al. (2012) Annulus fibrosus tissue engineering using lamellar silk scaffolds. *J Tissue Eng Regen Med* 6(Suppl 3):s24–s33.
4. Shao X, Hunter CJ (2007) Developing an alginate/chitosan hybrid fiber scaffold for annulus fibrosus cells. *J Biomed Mater Res A* 82:701–710.
5. Wan Y, Feng G, Shen FH, Laurencin CT, Li X (2008) Biphasic scaffold for annulus fibrosus tissue regeneration. *Biomaterials* 29:643–652.
6. Park S-H, et al. (2012) Intervertebral disk tissue engineering using biphasic silk composite scaffolds. *Tissue Eng Part A* 18:447–458.
7. Bhattacharjee M, Chameettachal S, Pahwa S, Ray AR, Ghosh S (2014) Strategies for replicating anatomical cartilaginous tissue gradient in engineered intervertebral disc. *ACS Appl Mater Interfaces* 6:183–193.
8. Bhattacharjee M, et al. (2012) Oriented lamellar silk fibrous scaffolds to drive cartilage matrix orientation: Towards annulus fibrosus tissue engineering. *Acta Biomater* 8: 3313–3325.
9. Bhattacharjee M, et al. (2016) Role of chondroitin sulphate tethered silk scaffold in cartilaginous disc tissue regeneration. *Biomed Mater* 11:025014.
10. Arai T, Freddi G, Innocenti R, Tsukada M (2004) Biodegradation of Bombyx mori silk fibroin fibers and films. *J Appl Polym Sci* 91:2383–2390.
11. Liu B, et al. (2015) Silk structure and degradation. *Colloids Surf B Biointerfaces* 131: 122–128.
12. Baker BM, et al. (2008) The potential to improve cell infiltration in composite fiber-aligned electrospun scaffolds by the selective removal of sacrificial fibers. *Biomaterials* 29:2348–2358.
13. Nerurkar NL, et al. (2009) Nanofibrous biologic laminates replicate the form and function of the annulus fibrosus. *Nat Mater* 8:986–992.
14. Mandal BB, Gil ES, Panilaitis B, Kaplan DL (2013) Laminar silk scaffolds for aligned tissue fabrication. *Macromol Biosci* 13:48–58.
15. Best BA, et al. (1994) Compressive mechanical properties of the human anulus fibrosus and their relationship to biochemical composition. *Spine* 19:212–221.
16. Yao H, Justiz M-A, Flagler D, Gu WY (2002) Effects of swelling pressure and hydraulic permeability on dynamic compressive behavior of lumbar annulus fibrosus. *Ann Biomed Eng* 30:1234–1241.
17. Antoniou J, et al. (1996) The human lumbar intervertebral disc: Evidence for changes in the biosynthesis and denaturation of the extracellular matrix with growth, maturation, ageing, and degeneration. *J Clin Invest* 98:996–1003.
18. Wu J, Cao W, Wen W, Chang DC, Sheng P (2009) Polydimethylsiloxane microfluidic chip with integrated microheater and thermal sensor. *Biomicrofluidics* 3:12005.
19. Mandal BB, Kundu SC (2008) Non-bioengineered silk fibroin protein 3D scaffolds for potential biotechnological and tissue engineering applications. *Macromol Biosci* 8: 807–818.
20. Iatridis JC (2009) Tissue engineering: Function follows form. *Nat Mater* 8:923–924.
21. Mandal BB, Grinberg A, Gil ES, Panilaitis B, Kaplan DL (2012) High-strength silk protein scaffolds for bone repair. *Proc Natl Acad Sci USA* 109:7699–7704.
22. Wei A, Shen B, Williams L, Diwan A (2014) Mesenchymal stem cells: Potential application in intervertebral disc regeneration. *Transl Pediatr* 3:71–90.
23. Mehlhorn AT, et al. (2006) Mesenchymal stem cells maintain TGF-β-mediated chondrogenic phenotype in alginate bead culture. *Tissue Eng* 12:1393–1403.
24. Gruber HE, et al. (1997) Human intervertebral disc cells from the annulus: Three-dimensional culture in agarose or alginate and responsiveness to TGF-β1. *Exp Cell Res* 235:13–21.
25. Awad HA, Halvorsen Y-DC, Gimble JM, Guilak F (2003) Effects of transforming growth factor β1 and dexamethasone on the growth and chondrogenic differentiation of adipose-derived stromal cells. *Tissue Eng* 9:1301–1312.
26. Anderson JM (2004) Inflammation, wound healing, and the foreign-body response. *Biomaterials Science: An Introduction to Materials in Medicine*, eds Ratner B, Hoffman A, Schoen F, Lemons J (Academic, New York), pp 296–304.

Downloaded at Palestinian Territory, occupied on December 7, 2021
www.manaraa.com